Application of Model-based LPV actuator fault estimation for an Industrial benchmark

Lejun Chen[a,*], Ron Patton[b], Philippe Goupil[c]

[a]*College of Engineering, Mathematics and Physical Sciences, University of Exeter, Exeter, UK, EX4 4QF*
[b]*School of Engineering, University of Hull, Hull, UK, HU6 7RX*
[c]*Flight Control System, Airbus Operations S.A.S. 316, Route de Bayonne 31060 Toulouse Cedex 09*

Abstract

To bridge the gap between model-based fault diagnosis theory and industrial practice, a linear parameter varying $\mathscr{H}_-/\mathscr{H}_\infty$ fault estimation approach is applied to a high fidelity nonlinear aircraft benchmark. The aim is to show how the fault estimation can provide robust early warning of actuator fault detection scenarios that can lead to abnormal aircraft flight configurations. The fault estimator state space solution is parameterized *a priori* using parameter-independent design freedom. Following this only constant free matrices are determined and the resulting affine linear parameter varying estimator has low computational load. The evaluation uses parametric simulation via an industry standard Monte Carlo campaign supported by a functional engineering simulator. The simulations are carried out in the presence of aerodynamic database uncertainties and measurement errors covering a wide range of the flight envelope.

Keywords: Fault estimation, $\mathscr{H}_-/\mathscr{H}_\infty$ optimisation, fault detection and diagnosis

*Corresponding author. Tel: +44-1392-723657
Email addresses: lejun.chen@exeter.ac.uk (Lejun Chen),
r.j.patton@hull.ac.uk (Ron Patton), philippe.goupil@airbus.com (Philippe Goupil)

1. Introduction

In the academic community, the methodologies of model-based fault detection and diagnosis (FDD) have been widely developed in last two decades (Patton, Frank & Clark, 1989, 2000; Isermann, 1997; Gertler, 1998; Chen & Patton, 1999; Isermann, 2005; Ding, 2008; Bokor & Szabo, 2009; Korbicz, Koscielny, Kowalczuk & Cholewa, 2004; Witczak, 2014) and some of them have been successfully applied to aeronautical and aerospace missions (Edwards, Lombaerts & Smaili, 2010) and have even been implemented in the Airbus industry practice to detect the oscillatory failure (Goupil, 2010; Lavigne et al., 2011). Recently, the application of linear parameter varying (LPV) concepts to system modelling, control and FDD have also received much attention (Balas, 2002; Bokor & Balas, 2004; Henry, 2008; Sato, 2010; Wei & Verhaegen, 2011a; Hecker & Pfifer, 2014; Alwi & Edwards, 2014; Henry et al., 2014; Varga & Ossmann, 2014; Vanek et al., 2014; Chen et al., 2016; Rodonto et al., 2015; Ossmann & Varga, 2015; Rotondo et al., 2015; Alwi et al., 2015). Nevertheless, the technical demands of model-based FDD, especially for the FDD problem based on using LPV, are still quite limited and restrictive in the aerospace industry (Zolghadri, 2012).

As a leading-edge European aerospace FDD project, the EU-FP7 funded ADDSAFE (Advanced Fault Diagnosis for Sustainable Flight Guidance and Control) bridges a gap between the advanced model-based FDD being developed by the academic community and technical solutions demanded by the aerospace industry. The ADDSAFE project benchmark was provided to several academic and industrial partners involved in this project to evaluate the efficiency of their FDD approaches on various fault scenarios (Alwi & Edwards, 2014; Henry et al., 2014; Varga & Ossmann, 2014; Vanek et al., 2014; Van Eykeren & Chu, 2014). The benchmark model is highly representative of a generic twin engine civil commercial aircraft including the nonlinear rigid-body aircraft model with a full set of control surfaces, actuator models, sensor models, flight control laws and pilot inputs. The aim of the project is to highlight the link between commercial aircraft sustainability and fault detection, it can be demonstrated that improving the fault diagnosis performance in flight control systems facilitates the optimization of the aircraft structural design (resulting in weight saving), which in turn helps to improve aircraft performance and to decrease its environmental footprint (e.g. fuel consumption and noise)(Goupil & Marcos, 2014).

In this paper, an LPV $\mathscr{H}_-/\mathscr{H}_\infty$ fault estimation approach is used to

provide the technical solution for the industrial benchmark scenarios. This approach has been widely developed in the literature (Ding et al., 2000; Wang et al., 2007; Henry & Zolghadri, 2005; Li et al., 2012; Grenaille et al., 2008; Henry, 2012), based on the original work by Hou & Patton (1997). There have been a number of application studies on aircraft flight control involving the generation of FDD residuals which are robust against modelling uncertainty, gust and turbulence (Marcos et al., 2005; Marcos & Balas, 2005; Yang & Wang, 2010; Wei & Verhaegen, 2011b; Li et al., 2012). The purpose of involving the $\mathcal{H}_-$ index in an $\mathcal{H}_\infty$ optimisation is to establish a trade-off between the fault sensitivity and the robustness of the residual Hou & Patton (1997). This paper extends the work in Li et al. (2012) into an LPV framework and proposes a specific $\mathcal{H}_-$ index which allows the fault estimation to be achieved in the presence of parametric uncertainties. The parameterizable solution of the fault estimator is then used to construct an $\mathcal{H}_\infty$ optimisation procedure.

The main motivation of the paper is to bridge the gap between the LPV $\mathcal{H}_-/\mathcal{H}_\infty$ approach and the technical solution required by the industry. The fault scenario 'Aircraft Abnormal Configuration' (Goupil & Marcos, 2014) is selected to be dealt with and the LPV fault estimation approach is implemented at both the local actuator model level and the global system level, to estimate various actuator jamming (also known as lock-in-place failure), those are 'liquid' jamming, 'solid' jamming and the control surface disconnection. The state space solution of the fault estimator is parameterised using *a priori* parameter-independent design freedom, and therefore only constant free matrices are computed. Compared with the polytopic LPV design approach, where gain matrices with respect to all vertices are required to be calculated and implemented, an affine LPV fault estimator can be implemented straightforwardly based upon using the free matrices, which largely reduces the computational load. Once the faults are estimated or detected in the presence of the parametric uncertainties caused by plant-model mismatch, aerodynamic database uncertainties, sensor noise and imperfect measurements of the scheduling parameters, the faulty actuator can be replaced by the adjacent redundant actuator at a very early stage of each fault development, and hence avoid the aircraft abnormal configuration. Furthermore, for the purpose of evaluating the design computational load, the fault estimator is recoded using the Airbus Flight Control Computer (FCC) software library. The fault estimation/detection results shown in this paper are evaluated based upon the parametric simulation and the Monte Carlo campaign

3

supported by an industrial functional engineering simulator.

The remainder of the paper is outlined as follows: Section 2 introduces the selected ADDSAFE fault scenario to be solved. The LPV modelling encompasses both local and global levels, as discussed in Section 3. Section 4 outlines the LPV $\mathscr{H}_-/\mathscr{H}_\infty$ approach. In Section 5 the ADDSAFE project verification process and industrial limitations are discussed. The parametric and Monte Carlo verification results are given in Section 6.

1.1. Notation

For a matrix X, $X < 0$ denotes that X is negative definite. X^T, X^{-1} and $X^\dagger$ denote its transpose, inverse and pseudo-inverse respectively. He$\{X\}$ denotes a shorthand notation for $X + X^T$ and $*$ denotes the symmetric entries of a matrix. Let an LPV system to be denoted in boldface upper case, for example, a parameter dependent system $\mathbf{G}_{uy}(\rho) : u \mapsto y$ indicates $y(s) = G(s, \rho)u(s)$ where ρ is the time-varying scheduling parameter. $\|v\|_2$ denotes the frequency domain 2-norm of the signal v. $\mathcal{L}_{2,\Omega}$ is the Lebesgue 2-space, wherein the signal is square integrable and norm bounded in a given finite frequency domain Ω, given by

$$\mathcal{L}_{2,\Omega} = \{v : \|v\|_{2,\Omega} < \infty\} \tag{1}$$

where $\|v\|_{2,\Omega}^2 = \frac{1}{2\pi} \int_\Omega v'(-j\omega)v(j\omega)d\omega$. The Lebesgue 2-space becomes infinite-horizon when $\Omega = [-\infty, \infty]$.

The frequency-domain $\mathscr{H}_\infty$ performance and $\mathscr{H}_-$ index for an LPV system $\mathbf{G}(\rho)$, appropriate to a given finite frequency range Ω, are defined by

$$\|\mathbf{G}(\rho)\|_{\infty,\Omega} = \sup_{\forall\rho\in\Theta,\forall u\in\mathcal{L}_{2,\Omega}} \frac{\|\mathbf{G}(\rho)u\|_{2,\Omega}}{\|u\|_{2,\Omega}}, u \neq 0 \tag{2}$$

$$\|\mathbf{G}(\rho)\|_{-,\Omega} = \inf_{\forall\rho\in\Theta,\forall u\in\mathcal{L}_{2,\Omega}} \frac{\|\mathbf{G}(\rho)u\|_{2,\Omega}}{\|u\|_{2,\Omega}}, u \neq 0 \tag{3}$$

2. ADDSAFE benchmark

2.1. Fault scenario: Aircraft Abnormal Configuration

The Aircraft Abnormal Configuration scenario is defined within the ADDSAFE benchmark, which concerns the detection of abnormal aircraft behaviour
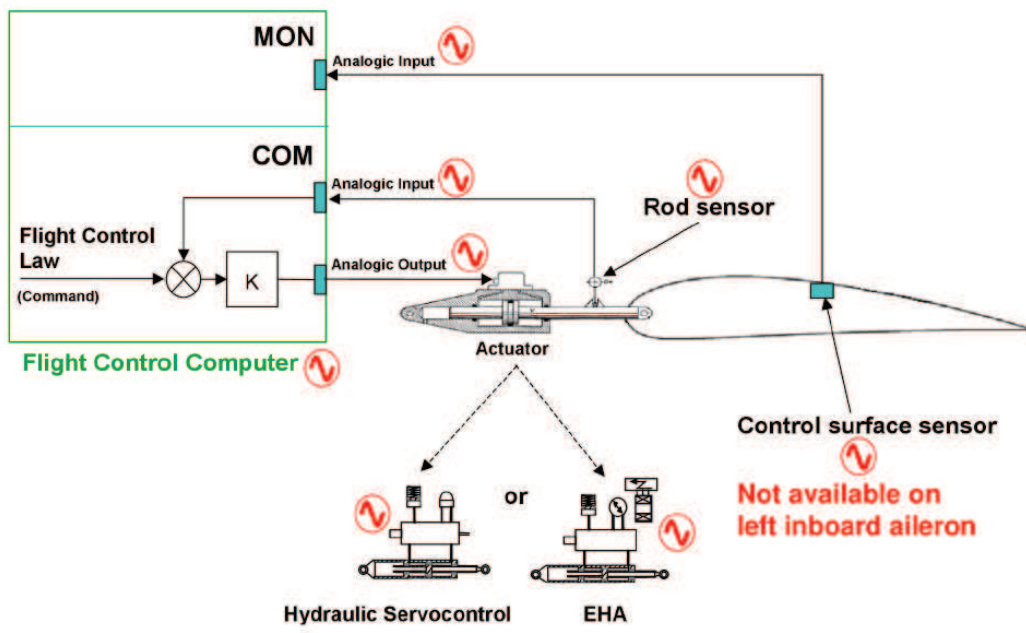
4

Figure 1: The locations of the actuator faults (Goupil, 2010)

caused by an actuator or sensor fault in the control loop of a control surface, between the FCC and the appropriate moving surfaces. The possible locations of the actuator faults are listed in Fig. 1.

In this paper, three fault sub-scenarios are selected to be solved from the standpoint of rapid and robust fault detection, these are:

- 'Liquid' jamming: A bias fault occurs on the left inboard aileron rod sensor.

- 'Solid' jamming: The left inboard aileron control surface is jammed at a fixed position.

- The control surface of the left inboard aileron is disconnected: A mechanical breakage occurs between the control surface and the actuator rod. Furthermore, the control surface sensor of the left inboard aileron is not necessarily available on all types of the aircraft.

The above fault sub-scenarios all lead to a control surface stuck at a fixed position. In current industrial state-of-practice, if the fault is not detected, it will trigger abnormal aircraft configurations, followed by deflection of other control surfaces to compensate for the effects of the faults, leading to the possibility of excessive fuel consumption. In addition, the compensation commands, corrupted by the faults, also become unreliable. For instance, a control surface jamming occurring on a spoiler or an aileron (as shown in the left hand side of the Fig. 2 will result in constant sideslip and roll rates. This will then raise the deflections of other control surfaces to compensate the asymmetric aircraft motion (as illustrated in the right hand side of Fig. 2).

The current AIRBUS state of practice is to use a dual active/passive scheme, i.e. an active actuator moving the control surface and adjacent passive actuator in a stand-by mode. So, if there exists a sufficiently early and precise fault estimation/detection, the faulty actuator can be switched off and the adjacent passive actuator becomes active. This provides an opportunity for the flight system to avoid the abnormal flight configuration.

In this work, 'liquid' and 'solid' jamming are modeled as additive sensor faults acting on the local aileron rod measurements, according to

$$
\begin{cases}
y = x & \text{fault-free case} \\
y = x + f_{liq} & \text{liquid jamming} \\
y = x + f_{sol}(x) & \text{solid jamming}
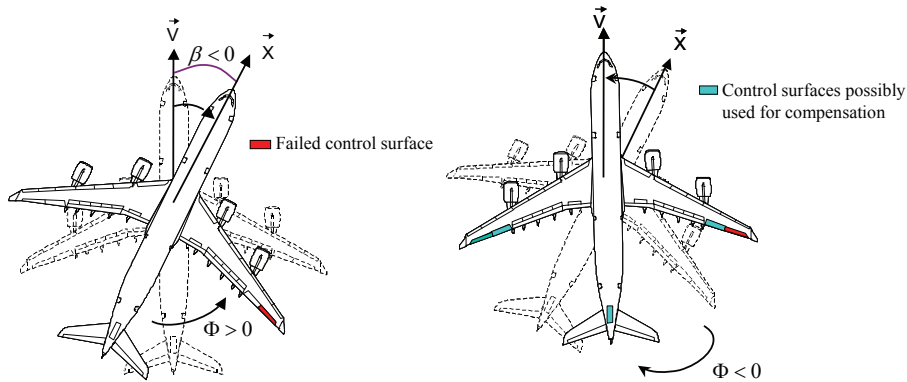\end{cases}
\tag{4}
$$

6

Figure 2: Effect of the dissymmetry (left hand side) and control surfaces used to compensate (right hand side)(Goupil, 2010)

where y are the outputs of the rod sensors and x are fault-free rod sensor outputs. f_{liq} represents additive 'liquid' jamming and $f_{sol}(x)$ represents the additive effect of 'solid' jamming. Note that $f_{sol}(x)$ is a function of x due to the occurrence of 'solid' jamming and in this situation the sensor measurements y are always stuck at fixed values.

Since there is no available control surface sensor on the left inboard aileron, aileron surface disconnection jamming is modeled as an additive actuator fault acting on the global model (including the aircraft rigid-body axis dynamics), according to:

$$\begin{cases} u = u_0 & \text{fault-free case} \\ u = u_0 + f_{dis} & \text{control surface disconnection} \end{cases} \tag{5}$$

where u denotes the control surface deflection signal, available from rod sensor outputs and f_{dis} represents the additive effect of the control surface disconnection. u_0 denotes the control surface deflection in the fault-free case.

In this paper, the proposed fault estimation approach is used to estimate the 'liquid' and 'solid' jamming faults at the local level (i.e. the fault estimation approach is applied to a local aileron component). The control surface disconnection is estimated at the global level (i.e. the fault estimation approach is applied to the global system level comprising the aircraft body axis model) due to the lack of an aileron surface sensor.

7

3. ADDSAFE LPV model in local and global levels

A benchmark system that is highly representative generic model of a twin engine civil commercial aircraft is defined within the ADDSAFE benchmark, which contains the nonlinear aircraft rigid-body model, flight control laws, pilot inputs and a full set of actuator and sensor dynamic models (Goupil & Puyou, 2011).

3.1. Global LPV model

In the ADDSAFE project, the LPV aircraft rigid-body model is built in an affine manner, based on using a multivariate least-squares approximation strategy (Hecker & Pfifer, 2014). This approach interpolates the multiple linear time invariant models linearised at various flight points in the flight envelope. This is effectively the affine state-space LPV model of the aircraft system used in the fault scenario study. In particular:

$$A(\rho) = A_0 + A_1 \rho_1 + \cdots + A_{n_\rho} \rho_{n_\rho} \tag{6}$$

The selected scheduling parameters are given by

$$\rho = [m(kg), X_{cg}(\%), V_{cas}(kt), h(ft)] \tag{7}$$

where, m is the weight of the aircraft, X_{cg} is the x-axis center gravity, V_{cas} denotes the calibrated airspeed and h is the altitude. Note that the angle of attack and load factor are assumed to be faulty in other ADDSAFE scenarios, and therefore they are not selected as the scheduling parameters. It must be stated that above selected scheduling parameters are independent from each other. Hence, the scheduling parameters vary inside a hyper-rectangle and satisfy the vertex property (Apkarian et al., 1995). Let $v_1, v_2, \ldots, v_r$ denote the vertices of the hyper-rectangle, say Θ, it follows

$$\rho \in \Theta \subset \mathbb{R}^{n_\rho} := Co\{\nu_1, \nu_2, \ldots, \nu_r, r = 2^{n_\rho}\} \tag{8}$$

and

$$A(\rho) = \sum_{i=1}^{r} \alpha_i(\rho) A(\nu_i), \quad \sum_{i=1}^{r} \alpha_i(\rho) = 1, \quad \alpha_i(\rho) \geq 0 \tag{9}$$

At the global level, the LPV model of the lateral aircraft rigid-body axis system is given by

$$\begin{aligned} \dot{x}_b &= A_b(\rho)x_b + B_b(\rho)u_b \\ y_b &= C_b x_b \end{aligned} \tag{10}$$

8

where y_b and x_b represent the aircraft lateral outputs and states, respectively. u_b includes the set of lateral actuator rod measurements together with a horizontal wind speed input along the aircraft body axis u_w[1].

3.2. Local quasi-LPV model

At the local actuator level, the first order dynamic of each of the simplified nonlinear servo-controller hydraulic aileron actuators (Goupil, 2010) is given by

$$\dot{x} = K_{ci}K_p(u - x)\sqrt{\frac{\delta P - \frac{F_{aero}+F_{damping}}{S}}{\delta P_{ref}}} \tag{11}$$

where, u is the commanded rod position and x is the hydraulic actuator rod position. The gain K_{ci} corresponds to the servo valve conversion of estimated current to the rod speed for each actuator and K_p is the servo control gain. δP is the hydraulic pressure delivered to the actuator. δP_{ref} is the constant differential pressure with the servo valve fully opened. F_{aero} represents the aerodynamic forces acting on the control surface. S is the actuator piston surface area. $F_{damping}$ represents the servo-control load of the adjacent actuator in damping mode.

The local quasi-LPV formulation of Eq. (11) is established by Hecker & Pfifer (2014):

$$\dot{x} = -K(\rho, x, sign(\dot{x}))x + K(\rho, x, sign(\dot{x}))u \tag{12}$$

where ρ is defined in Eq. (7) and

$$K(\rho, x, sign(\dot{x})) = C_0(\rho) + C_1(\rho)sign(\dot{x})(x + C_2(\rho)) \tag{13}$$

where $C_0(\rho)$, $C_1(\rho)$ and $C_2(\rho)$ depend affinely on ρ, and this dependence is calculated using a parameter fitting approach based on comparing the output responses of the nonlinear actuator model and LPV model. In (12), $sign(\dot{x})$ is a function of the deflection rate, which is used to distinguish the upward and downward movements of the control surface when $\dot{x} \neq 0$, given by

$$sign(\dot{x}) = \begin{cases} 1 & \text{if } \dot{x} > 0 \\ 0 & \text{if } \dot{x} = 0 \\ -1 & \text{if } \dot{x} < 0 \end{cases} \tag{14}$$

---

[1]In ADDSAFE, the wind effect is not taken into account (i.e. $u_w = 0$)

In the situation $\dot{x} = 0$, the control surface does not move. The aerodynamic force acting on the control surface is fixed at given specific flight condition. Also, there is no further upward or downward deflection is commanded, the actuator does not have to work against the disturbing aerodynamic force and therefore the dynamic is fixed at a given flight point.

4. LPV $\mathscr{H}_-/\mathscr{H}_\infty$ Fault Estimation

Consider an affine LPV system subject to actuator and sensor faults and parametric uncertainties, given by

$$
\begin{aligned}
\dot{x} &= A(\rho)x + B(\rho)u + F(\rho)f + M(\rho)\delta \\
y &= C(\rho)x + D(\rho)u + H(\rho)f + N(\rho)\delta
\end{aligned}
\tag{15}
$$

where, x, u, and y represent the system states, inputs and outputs respectively. $f \in \mathcal{L}_{2,\Omega}$ denotes the sensor or actuator fault or a combination of sensor and actuator faults. $\delta \in \mathcal{L}_{2,\Omega}$ represents the parametric uncertainties. As defined in Eq. (8), the scheduling parameters ρ are assumed to vary in a polytope Θ. All parameter-dependent matrices in Eq. (15) are assumed to depend affinely on ρ (as shown in Eq. (6)) and satisfy the vertex property (as shown in Eq. (9)). Provided that the sensor fault is additive, $H(\rho)$ becomes a fixed matrix, i.e. $H(\rho) = H$.

Assumption 4.1. *(i) $(C(\rho), A(\rho))$ is detectable, $\forall \rho \in \Theta$. (ii) Matrix H is full column rank. (iii) $\mathbf{G}_{fy}(\rho) : f \mapsto y$ has no zeros on the extended imaginary axis, $\forall \rho \in \Theta$.*

Remark 4.1. *In Assumption 4.1, (i) guarantees that, $\forall \rho \in \Theta$, there exists $L(\rho)$ such that $A(\rho) + L(\rho)C(\rho)$ is negative, which can be verified using the vertex property. (ii) is necessary for the existence of the solution of the LPV fault estimator, which is relaxed by Wang & Yang (2008). For the actuator disconnection failure case, H is not full column rank and a small perturbation matrix can be used to perturb H to fulfill the full column requirement (Wang et al., 2007; Li & Zhou, 2009). (iii) is necessary for the existence of a stable fault estimator.*

The proposed fault estimator is given by

$$
\begin{aligned}
\dot{\hat{x}} &= A(\rho)\hat{x} + B(\rho)u - L_1(\rho)(y - \hat{y}) \\
\hat{y} &= C(\rho)\hat{x} + D(\rho)u \\
\hat{f} &= L_2(y - \hat{y})
\end{aligned}
\tag{16}
$$

where $L_1(\rho)$ and L_2 are estimator gains. $\hat{y}$ denotes the observer outputs and $\hat{f}$ represents the fault estimate. Let $e = x - \hat{x}$, the error dynamics between observer and plant are given by

$$\begin{aligned}
\dot{e} =& (A(\rho) + L_1(\rho)C(\rho))e + (F(\rho) + L_1(\rho)H)f + (M(\rho) + L_1(\rho)N(\rho))\delta \\
\hat{f} =& L_2 C(\rho)e + L_2 H f + L_2 N(\rho)\delta
\end{aligned}$$
(17)

Since an ideal fault estimator requires $\mathbf{G}_{\hat{f}f}(\rho) = \mathbf{I}$, where $\mathbf{G}_{\hat{f}f}(\rho) : \hat{f} \mapsto f$. This is equivalent to finding a fault estimator to achieve a specific $\mathscr{H}_-$ index $\|\mathbf{G}_{\hat{f}f}(\rho)\|_- \geq 1$ since $\|\mathbf{I}\|_- \geq 1$. The robust fault estimation problem can now be formulated as an $\mathscr{H}_-/\mathscr{H}_\infty$ problem:

Problem 4.1. *Given a system in Eq.(15), find a stable robust fault estimator with gain matrices $L_1(\rho)$ and L_2 to generate a fault estimate $\hat{f}$, achieving the following infimum:*

$$\gamma := \inf_{\forall \rho \in \Theta} \{\|\mathbf{G}_{\hat{f}\delta}(\rho)\|_{\infty,\Omega} : \|\mathbf{G}_{\hat{f}f}(\rho)\|_{-,\Omega} \geq 1\} \tag{18}$$

According to Chen et al. (2016), Eq. (18) is also equivalent to

$$\gamma := \inf_{\forall \rho \in \Theta} \{\|\mathbf{G}_{\hat{f}\delta}(\rho)\|_{\infty,\Omega} : \mathbf{G}_{\hat{f}f}(\rho) = \mathbf{I}\} \tag{19}$$

Since $L_2 \neq 0$, the necessary and sufficient condition to achieve $\mathbf{G}_{\hat{f}f}(\rho) = \mathbf{I}$ is that both $F(\rho) + L_1(\rho)H = 0$ and $L_2 H = I$ are satisfied for any $\rho \in \Theta$. It follows from the work in Li et al. (2012) and Chen et al. (2016) that the corresponding solutions of $L_1(\rho)$ and L_2 are given by

$$L_1(\rho) = -F(\rho)H^\dagger + Z_1 H^\perp \tag{20}$$

$$L_2 = H^\dagger + Z_2 D_f^\perp \tag{21}$$

where Z_1 and Z_2 are design matrices to be calculated to achieve fault estimation. Substituting Eq. (20) and Eq. (21) into the error dynamic in Eq. (17), the $\mathscr{H}_-/\mathscr{H}_\infty$ performance γ in in Eq.(19) can be achieved via finding a symmetric positive definite matrix P, full matrix Z_1 and Z_2, such that

$$\begin{bmatrix} \text{He}\{P(A(\rho) - F(\rho)H^\dagger C(\rho) + Z_1 H^\perp C(\rho))\} & * & * \\ P(M(\rho) - F(\rho)H^\dagger N(\rho) + Z_1 H^\perp N(\rho)) & -\gamma I & * \\ (H^\dagger + Z_2 H^\perp)C(\rho) & (H^\dagger + Z_2 H^\perp)N(\rho) & -\gamma I \end{bmatrix} < 0$$
(22)

11

It is clear that the above matrix inequality is not convex. According to the vertex property (Apkarian et al. (1995)), solving the matrix inequality is equivalent to finding a symmetric positive definite matrix P, full matrix S and Z_2, such that, for all $i, j \in 1, 2, \cdots, r$:

$$\begin{bmatrix} \text{He}\{PA(\nu_i) - PF(\nu_j)H^\dagger C(\nu_i) + SH^\perp C(\nu_i)\} & * & * \\ PM(\nu_i) - PF(\nu_j)H^\dagger N(\nu_i) + SH^\perp C(\nu_i) & -\gamma I & * \\ (H^\dagger + Z_2 H^\perp)C(\nu_i) & (H^\dagger + Z_2 H^\perp)N(\nu_i) & -\gamma I \end{bmatrix} < 0$$

$$(23)$$

Then the matrix Z_1 can be calculated via $Z_1 = P^{-1}S$. After solving both Z_1 and Z_2, the fault estimator gains $L_1(\rho)$ and L_2 can be solved directly using Eq. (20) and Eq. (21) rather than calculating polytopic gains. Note that the resulting estimator gains may not always stabilize the fault estimator. An inner-outer factorization has to be performed and the fault estimation performance will be scarified, which is not discussed in this paper.

Note that the work in this paper is different from one presented in Chen et al. (2016). In Chen et al. (2016), sensor faults are estimated based upon using an LPV reference model and the robustness of the fault estimation is ensured by minimising the distance between the actual fault estimation and one from the reference design. The method in Chen et al. (2016) contains two steps and relies on an ideal reference solution to be calculated in the first step. In this paper, a fault estimator is calculated straightforwardly in one step and therefore an ideal reference solution is not required.

5. Performance Evaluation

5.1. Parametric simulation

The robustness of the fault estimation/detection will be evaluated over the whole flight envelope with various measurements and aerodynamic database uncertainties. During the evaluation process, a parametric simulation is run to provide an initial robustness verification based on multiple fixed flight conditions inside the flight envelope (listed in Table 1). The units of the flight conditions are fixed in the ADDSAFE project.

For each of the simulation flight conditions in the flight envelope, error bounds on the uncertain aerodynamic parameters, sensor measurements and estimation of physical parameters are applied, according to the information given in Table 2.

Table 1: Multiple flight conditions inside flight envelope chosen for parametric simulation

Parameter	flight conditions			
Altitude (ft$\times 10^3$)	8	18	28	38
Calibrated airspeed (kts)	160	220	300	
Mass (ton)	120	180	233	
Center of gravity (%)	17	30	41	

Table 2: Aerodynamic database uncertainty bounds, sensor measurements and estimation

Parameter	Variable	Min		Max
Aerodynamic coefficients	$\delta C_x, \delta C_y, \delta C_z$ $\delta C_l, \delta C_m, \delta C_n$	-5%	0	5%
Measurements	$\delta V_{cas}, \delta h$	-10%	0	10%
Estimation	$\delta m, \delta X_{cg}$	-10%	0	10%

Clearly, after combining four altitude values, three various values of calibrated airspeeds, mass and center of gravity, and the upper and lower uncertainty bounds of uncertainty listed in Table 1 and Table 2, for each fault sub-scenario, a parametric simulation will cover 324 grid points. Among 324 points, 158 flight points correspond most closely to realistic flight behaviour are selected for the parametric validation.

5.2. Industrial Monte-Carlo Campaign

The Monte Carlo campaign is run by the industry, based upon statistical sampling of the flight conditions within the bound of the flight envelope, according to a suitable probability distribution.

For the Monte Carlo simulation campaign, 1200 fault-free runs are distributed evenly (i.e. 200 each) among six benchmark-defined flight manoeuvres which will be discussed later. Then 1000 runs are distributed evenly among the different types of faults applicable to the fault scenario (e.g. 333 runs for 'liquid' jamming, 333 runs for 'solid' jamming and 334 runs for control surface disconnection).

5.3. Evaluation Tools: Functional Engineering Simulator

The performance robustness of the proposed fault estimator is evaluated using the Functional Engineering Simulator (FES). FES is a term used in Space Systems Engineering to describe a software simulator describing the

components of a system (including its operating environment) at a functional level. FES systems are used in support of the specification, design, verification and operations of space systems, and can be used across the spacecraft development life-cycle, including activities such as system design validation, software verification and validation, spacecraft unit and sub-system test activities (Fernandez et al., 2010). The FES developed by Deimos Space S.L.U. for the ADDSAFE project (Fernandez & Ramon, 2011) is a non-real-time simulator based on Simulink, Matlab and XML that includes the Airbus benchmark model as well as the robustness and performances metrics for all the fault scenarios defined in the project (Goupil & Marcos, 2012). In ADDSAFE project, both the parametric simulation or the Monte-Carlo campaign are run based upon using FES. In addition, the predefined evaluation metrics, for instance, detection time performance (DTP), false alarm rate (FA), missed detection rate (MD) will be calculated by FES.

5.4. Industrial Limitation and Constraints

On a large civil aircraft, the computing capability of the FCC is low and the proven and robust processors must be used for critical applications. Therefore, it is hard to use advanced processing with high computational load, like on-line optimisation or even wavelet or Fourier transforms.

In ADDSAFE project, to facilitate the industrial evaluation of the computational load of the design, the fault estimation algorithm is recoded purely based on the Airbus state of practice for the FCC software coding SAO (Airbus software, Computer-Assised Specifiation) library, which contains a set of graphical functional blocks in the manner of SIMULINK blocks, allowing only a limited set of mathematical operations. Then, an automatic generation tool is used to calculate the computational load and produce the code to be implemented in the FCC.

6. Benchmark results

Both the 'liquid' and 'solid' jamming faults are estimated at the local level, the corresponding quasi-LPV model is given by

$$
\begin{aligned}
\dot{x} &= -K(\rho, x, sign(\dot{x}))x + K(\rho, x, sign(\dot{x}))u + \delta_l(y, u, \rho) \\
y &= x + f_{jam}
\end{aligned}
\tag{24}
$$

where f_{jam} represents the jamming faults (f_{liq} or f_{sol}) in the rod sensor measurements. $\delta_l(y, u, \rho)$ represents the parametric uncertainties (defined

14

in Table 2) in a local level. A new scheduling parameter $\tilde{\rho}$ of the quasi-LPV model is defined, such that $\tilde{\rho} = \begin{bmatrix} \rho & x \end{bmatrix}^T$ and $sign(\dot{x})$ allow upward and downward movements of the control surfaces to be distinguished. More details of using the above quasi-LPV model in (24) to approximate actuator dynamics in (11) are discussed in Hecker & Pfifer (2014); Varga & Ossmann (2014); Ossmann & Varga (2015).

The effect of the control surface disconnection is estimated at the global level and the associated faulty LPV model is given by

$$
\begin{aligned}
\dot{x}_b &= A_b(\rho)x_b + B_b(\rho)u_b + B_b(\rho)W f_{dis} + M_g \delta_g(y, u, \rho) \\
y_b &= C_b x_b + H f_{dis}
\end{aligned}
\tag{25}
$$

where $y_b = \begin{bmatrix} \phi & p & r \end{bmatrix}^T$ and $x_b = \begin{bmatrix} \phi & v_y & p & r \end{bmatrix}^T$ represent the aircraft lateral outputs and states, respectively. ϕ and p denote the roll angle and roll rate, respectively. r is the yaw rate measurement and v_y is velocity of the aircraft along y-axis. u_b contains rod measurements of the four ailerons, eight spoilers and one rudder. f_{dis} represents the effect of the control surface disconnection. $\delta_g(y, u, \rho)$ represents the parametric uncertainty in a globe level and M_g denotes its distribution matrix. As argued in Wang et al. (2007); Li & Zhou (2009), H is chosen to be a small perturbation matrix to ensure it is full column rank. The value of M_g is obtained using a linear fractional transformation-based realization (Marcos et al., 2007). Furthermore, as argued by Alwi & Edwards (2014), parametric uncertainties δ_g mainly affect the channels with respect to the roll rate and the yaw rate. W is a diagonal semi-positive definite weighting matrix with diagonal elements representing the efficiency levels of corresponding control surfaces. For control surface disconnection, the diagonal element associated with left inboard aileron in W is '1', the other diagonal elements are set to be '0'.

The $\mathcal{H}_-/\mathcal{H}_\infty$ LPV fault estimation approach introduced in Section 4 is then applied to the local model and global model to estimate f_{jam} and f_{dis}, respectively. Note that in Eq. (24) and Eq. (25), the output matrices and the uncertainty distribution matrices are all constant. This largely reduces the design conservatism and only r LMIs are required to be solved to find P.

In this paper, the design results are not included due to the confidential requirements of the project. Therefore, only simulation results from the FES simulator are presented.

6.1. Fault free case

For ADDSAFE fault scenarios, a zero false alarm rate must be guaranteed in the fault-free situation. Here, six flight conditions or manoeuvres are chosen to be simulated as fault-free. These are: Nose up (abrupt longitudinal manoeuvre), Angle of attack (AOA) protection (triggering of angle of attack protection), Pitch protection (triggering of pitch protection), Yaw angle mode (corresponding to an enhanced auto-pilot hold mode), Turn coordination (coordinated turn) and Cruise phase. For each flight manoeuver, 158 and 200 runs are executed for the parametric and Monte Carlo simulations, respectively. During six flight manoeuvres in the fault-free case, residual signals associated with 'liquid' jamming, 'solid' jamming and the surface disconnection are shown in Figs. 3-8. The green lines in Figs. 3-8 represent values of constant thresholds. Clearly, in the fault-free case, residual signals do not trigger thresholds and the zero false alarm can be guaranteed. Note that the labelling of the y-axis is hidden from Figs. 3-8 due to the industrial limitation.

6.2. Inboard aileron failure case

In the aileron failure case, the aircraft is assumed to be in Cruise manoeuvre. Normalized Monte Carlo fault estimation and detection results associated with 'liquid' jamming, 'solid' jamming and the control surface disconnection scenarios are shown in Fig. 9, Fig. 10 and Fig. 11, respectively. In 'liquid' jamming, 'solid' jamming and control surface disconnection scenarios, the jamming represents 1.3%, 1.8% and 21.4% of the control surface deflection operational range, respectively. Figure. 9(a) shows demands of the left inboard aileron on various flight conditions and Fig. 9(b) depicts aileron rod sensor measures which are corrupted by 'liquid' jamming. Figure 9(c) shows fault estimates of 'liquid' jamming and it can be seen from Fig. 9(c) that estimated 'liquid' jamming occur around 11sec and then disappears. For the purpose of confirming the fault occurrence and reducing the effect of the spike raised during the Yaw angle mode manoeuvre in the fault-free case, a fixed post-filter is added, specifically for 'liquid' jamming, to reduce the effect of the spike, whilst maintaining both the amplitudes of the fault estimates and the effect of the bias. The transfer function of the post-filer is given by $T(s) = (s + 1)/(s + 5)$. Then an integrator is used to maintain the effect of the fault bias till the end of the simulation for the decision making purpose. The filtered fault estimates are shown in Fig. 9(d) wherein blue lines represent residuals in the presence of the parametric uncertainties and the

green line represents the value of the constant threshold used for detecting 'liquid' jamming. Fault estimation errors between fault estimates and faults on various flight conditions are shown in Fig. 9(e). Clearly from Fig. 9(e), fault estimation errors are close to zero despite various flight conditions and parametric uncertainties. The mean and variance of fault estimation errors in the presence of 'liquid' jamming are 0.0013 and $3.039e - 08$, respectively. Fault detection signals with respect to various flight conditions are shown in Fig. 9(f). In Fig. 9(f), changes of boolean signals from '0' to '1' represent the situations in which faults are detected and confirmed. It is clear that 'liquid' jamming can be detected rapidly despite all flight conditions.

Fault estimation and detection performance in the presence of 'solid' jamming are shown in Fig. 10. Figure 10(a) shows demands of the left inboard aileron on various flight conditions and aileron rod sensor measurements affected by 'solid' jamming are shown in Fig. 10(b). Blue lines in Fig. 10(c) depict fault estimates despite various flight conditions and parametric uncertainties and the green line represents the constant threshold. Fault estimation errors on various flight conditions are shown in Fig. 11(d). It is clear that fault estimation errors are close to zero and fault estimates correctly reconstruct faults despite parametric uncertainties. The mean and variance of fault estimation errors are 0.0014 and $2.7972e - 08$, respectively. It is also clear from Fig. 10(e) that, for all testing conditions, faults are detected immediately after their occurrence.

Figure 11 demonstrates fault estimation performance in the face of control surface disconnections. Figures 11(a) and 11(b) show left inboard aileron commands and their rod sensor measurements, respectively. It can be seen from Figs. 11(a) and 11(b) that the rod sensor is fault-free and therefore faults are chosen to be estimated at the global system level. Using the LPV observer proposed in this paper, fault estimates and fault detection signals despite various flight conditions and parametric uncertainties are shown in Fig. 11(c) and Fig. 11(e), respectively. Note that fault estimates in Fig. 11(c) are sparse compared with those shown in Fig. 10(c). This is because left inboard aileron commands in Fig. 11(a) are sparse when effected by surface disconnections. Clearly from Fig. 11(c), the fault estimator is stable and robust enough so that parametric uncertainties do not significantly reduce the estimation performance. The mean and variance of fault estimation errors in the presence of surface disconnections cannot be calculated straightforwardly due to the lack of the control surface sensor in the left inboard aileron and the knowledge of the additive effect of the disconnection f_{dis} is not available

from the FES.

The evaluation results of the parametric simulation and the Monte Carlo campaign, generated using FES, are shown in Tables 3 and 4, respectively. It is clear from Tables 3 and 4 that the false alarm rate (FA) and missed detection rate (MD) are zero despite various flight conditions and parametric uncertainties. The detection time performance (DTP) (the value '1' indicates that that the fault is detected at the required detection time and any values between '0' and '1' indicates a faster detection) is stable and low, which implies that all faults are detected rapidly.

7. Conclusion

In this paper, an $\mathscr{H}_-/\mathscr{H}_\infty$ LPV fault estimation approach is applied to deal with an industrial benchmark problem. The design computational load and the fault estimation performance are evaluated by Airbus, via using FCC software tools and the FES tool. The simulation results from the Monte Carlo campaign show the robustness of the fault estimation against the parametric uncertainties raised by plant-model mismatch, aerodynamic database uncertainties and physical parameter measurements errors. The future work is to evaluate the proposed scheme in the most recent EU-FP7 RECONFIGURE project (Goupil et al., 2014, 2015) wherein a larger range of flight conditions, more challenging fault detection/fault tolerant control scenarios and various flight manoeuvres including different wind profiles and turbulence are taken into account.

8. Acknowledgments

References

Alwi, H., & Edwards, C. (2014). Development and application of sliding mode LPV fault reconstruction schemes for the ADDSAFE. *Control Engineering Practice*, *31*, 148–170.

Table 3: Evaluation results for the parametric simulation

Fault scenario	Evaluation results		
	FA (%)	MD (%)	Min/Mean/Max DTP
'Liquid' jamming	0	0	0.00116667/0.00116667/0.00116667
'Solid' jamming	0	0	0.001/0.001/0.001
Control surface disconnection	0	0	0.00758333/0.0191682/0.0584167

Table 4: Evaluation results for the Monte Carlo campaign

Fault scenario	Evaluation results		
	FA (%)	MD (%)	Min/Mean/Max DTP
'Liquid' jamming	0	0	0.00116667/0.00116667/0.00116667
'Solid' jamming	0	0	0.001/0.001/0.001
Control surface disconnection	0	0	0.008/0.0152707/0.0376667

Alwi, H., Edwards, C., Stroosma, O., Mulder, J., & Hamayun, M. (2015). Real-time implementation of an ISM fault-tolerant control scheme for lpv plants. *IEEE Transactions on Industrial Electronics*, *62*, 3896–3905.

Apkarian, P., Gahinet, P., & Becker, G. (1995). Self-scheduled $\mathscr{H}_\infty$ control of linear parameter-varying systems: a design example. *Automatica*, *31(9)*, 1251–1261.

Balas, G. J. (2002). Linear, parameter-varying control and its application to a turbofan engine. *International Journal of robust and nonlinear control*, *12*, 763–796.

Bokor, J., & Balas, G. J. (2004). Detection filter design for LPV systems − a geometric approach. *Automatica*, *40(3)*, 511–518.

Bokor, J., & Szabo, Z. (2009). Fault detection and isolation in nonlinear systems. *Annual Reviews in Control*, *33*, 113–123.

Chen, J., & Patton, R. J. (1999). *Robust model-based fault diagnosis for dynamic systems*. Boston/Dordrecht/London. Kluwer Academic Publishers.

Chen, L., Patton, R., & Goupil, P. (2016). Robust fault estimation using an LPV reference model: ADDSAFE benchmark case study. *Control Engineering Practice*, *49*, 194–203.

Ding, S. X. (2008). *Model-based fault diagnosis techniques: Design schemes, algorithms, and tools*. Heidelberg, Berlin: Springer.

Ding, S. X., Jeinsch, T., Frank, P. M., & Ding, E. (2000). A unified approach to the optimization of fault detection systems. *Journal of Adaptive Control and Signal Processing*, *17(4)*, 725–745.

Edwards, C., Lombaerts, T., & Smaili, H. (2010). *Fault tolerant flight control: A benchmark challenge*. Springer.

Fernandez, V., De Zaiacomo, G., Mafficini, A., & Penin, L. F. (2010). The IXV GNC Functional Engineering Simulator. In *11th International Workshop on Simulation & EGSE facilities for Space Programmes*. ESA-ESTEC.

Fernandez, V., & Ramon, J. M. (2011). *FES software users manual, ADDSAFE Technical Note D1.2.1*. Technical Report DEIMOS.

Gertler, J. (1998). *Fault detection and diagnosis in engineering systems*. Marcel Dekker, Inc., New York.

Goupil, P. (2010). Oscillatory failure case detection in the A380 electrical flight control system by analytical redundancy. *Control Engineering Practice*, *18(9)*, 1110–1119.

Goupil, P., Boada-Bauxell, J., Marcos, A., Cortet, E., Kerr, M., & Costa, H. (2014). AIRBUS efforts toward advanced real-time fault diagnosis and fault tolerant control. In *19th IFAC World Congress*.

Goupil, P., Boada-Bauxell, J., Marcos, A., Rosa, P., Kerr, M., & Dalbies, L. (2015). An overview of the FP7 RECONFIGURE project: Industrial, scientific and technological objectives. In *SAFEPROCESS '15*.

Goupil, P., & Marcos, A. (2012). Industrial benchmarking and evaluation of ADDSAFE FDD design. In *IFAC SAFEPROCESS'12* (pp. 1131–1136). Mexico City volume 45.

Goupil, P., & Marcos, A. (2014). The European ADDSAFE project: Industrial and academic efforts towards advanced fault diagnosis. *Control Engineering Practice*, *31*, 109–125.

Goupil, P., & Puyou, G. (2011). A high fidelity AIRBUS benchmark for system fault detection and isolation and flight control law clearance. In *4th European Conference for Aerospace Sciences*. Saint Petersburg, Russia.

Grenaille, S., Henry, D., & Zolghadri, A. (2008). A method for designing fault diagnosis filters for LPV polytopic systems. *J. Control Sci. Eng.*, *2008*, 1:1–1:11.

Hecker, S., & Pfifer, H. (2014). Affine LPV-modeling for the ADDSAFE benchmark. *Control Engineering Practice*, *31*, 126–134.

Henry, D. (2008). Fault diagnosis of the MICROSCOPE satellite actuators using $\mathscr{H}_-/\mathscr{H}_\infty$ filters. *AIAA Journal of Guidance, Control and Dynamics*, *31(3)*, 699–711.

Henry, D. (2012). Structured fault detection filters for LPV systems modeled in an LFT manner. *International Journal of Adaptive Control and Signal Processing*, *26*, 190–207.

21

Henry, D., Cieslak, J., Zolghadri, A., & Efimov, D. (2014). A non-conservative solution for early and robust fault diagnosis in aircraft control surfaces servo-loops. *Control Engineering Practice*, *31*, 183–199.

Henry, D., & Zolghadri, A. (2005). Design and analysis of robust residual generations for systems under feedback control. *Automatica*, *41(2)*, 251–264.

Hou, M., & Patton, R. J. (1997). An $\mathscr{H}_-/\mathscr{H}_\infty$ approach to the design of robust fault diagnosis observers based upon LMI optimisation. In *Proceeding of the 4th European Control Conference*. Brussels, Belgium.

Isermann, R. (1997). Trends in the application of model-based fault detection and diagnosis of techinical process. *Control Engineering Practice*, *5(5)*, 709–719.

Isermann, R. (2005). Model-based fault-detection and diagnosis status and applications. *Annual Reviews in Control*, *29(1)*, 71–85.

Korbicz, J., Koscielny, J. M., Kowalczuk, Z., & Cholewa, W. (2004). *Fault Diagnosis. Models, Artificial Intelligence, Applications*. Springer-Verlag Berlin Heidelberg.

Lavigne, L., Zolghadri, A., Goupil, P., & Simon, P. (2011). A model-based technique for early and robust detection of oscillatory failure case in A380 actuators. *International Journal of Control, Automation and Systems*, *9*, 42–49.

Li, X., & Zhou, K. (2009). A time domain approach to robust fault detection of linear time-varying systems. *Automatica*, *45*, 94–102.

Li, Z., Mazars, E., Zhang, Z., & Jaimoukha, I. M. (2012). State-space solution to the $\mathscr{H}_-/\mathscr{H}_\infty$ fault-detection problem. *International Journal of Robust and Nonlinear Control*, *22*, 282–299.

Marcos, A., & Balas, G. J. (2005). A robust integrated controller/diagnosis aircraft application. *International journal of robust and nonlinear control*, *15(12)*, 531–551.

Marcos, A., Bates, D. G., & Postlethwaite, I. (2007). Nonlinear symbolic LFT tools for modeling, analysis and design. (pp. 69–92). Springer Berlin Heidelberg.

Marcos, A., Ganguli, S., & Balas, G. J. (2005). An application of $\mathcal{H}_\infty$ fault detection and isolation to a transport aircraft. *Control Engineering Practice*, *13(1)*, 105–119.

Ossmann, D., & Varga, A. (2015). Detection and identification of loss of efficiency faults of flight actuators. *Int. J. Appl. Math. Comput. Sci.*, *25*, 53–63.

Patton, R. J., Frank, P. M., & Clark, R. N. (1989). *Fault diagnosis in dynamic systems: Theory and application*. Prentice Hall, London.

Patton, R. J., Frank, P. M., & Clark, R. N. (2000). *Issues in fault diagnosis for dynamic systems*. Springer.

Rodonto, D., Nejjari, F., & Puig, V. (2015). Robust quasi-LPV model reference FTC of a quadrotor UAV subject to actuator faults. *International Journal of Applied Mathematics and Computer Sciences*, *25*, 7–22.

Rotondo, D., Puig, V., Nejjari, F., & J, R. (2015). A fault-hiding approach for the switching quasi-LPV fault-tolerant control of a four-wheeled omnidirectional mobile robot. *IEEE Transactions on Industrial Electronics*, *62*, 3932–3944.

Sato, M. (2010). Gain-scheduling open-loop system design for LPV systems using polynominally parameter-dependent Lyapunov functions. *Systems and Control Letters*, *59*, 265–276.

Van Eykeren, L., & Chu, P. (2014). Sensor fault detection and isolation for aircraft control systems by kinematic relations. *Control Engineering Practice*, *31*, 200–210.

Vanek, B., Edelmayer, A., Szabo, Z., & Bokor, J. (2014). Bridging the gap between theory and practice in lpv fault detection for flight control acuators. *Control Engineering Practice*, *31*, 171–182.

Varga, A., & Ossmann, D. (2014). LPV model-based robust diagnosis of flight actuator faults. *Control Engineering Practice*, *31*, 135–147.

Wang, H., & Yang, G. H. (2008). A finite frequency domain approach to fault detection for linear discrete-time systems. *International Journal of Control*, *87(7)*, 1162–1171.

Wang, J. L., Yang, G. H., & Liu, J. (2007). An LMI approach to $\mathcal{H}_-$ index and mixed $\mathcal{H}_-/\mathcal{H}_\infty$ fault detection observer design. *Automatica*, *43(9)*, 1656–1665.

Wei, X., & Verhaegen, M. (2011a). LMI solutions to the mixed $\mathcal{H}_-/\mathcal{H}_\infty$ fault detection observer design for linear parameter-varying systems. *International Journal of Adaptive Control and Signal Processing*, *25(2)*, 114–136.

Wei, X., & Verhaegen, M. (2011b). Robust fault detection observer design for linear uncertain systems. *International Journal of Control*, *84*, 197–215.

Witczak, M. (2014). *Fault diagnosis and fault-tolerant control strategies for non-linear systems*. Springer International Publishing.

Yang, G. H., & Wang, H. (2010). Fault detection for a class of uncertain state-feedback control systems. *IEEE Transactions on Control Systems Technology*, *18*, 201–212.

Zolghadri, A. (2012). Advanced model-based FDIR techniques for aerospace systems: Today challenges and opportunities. *Progress in Aerospace Sciences*, *53*, 18–29.
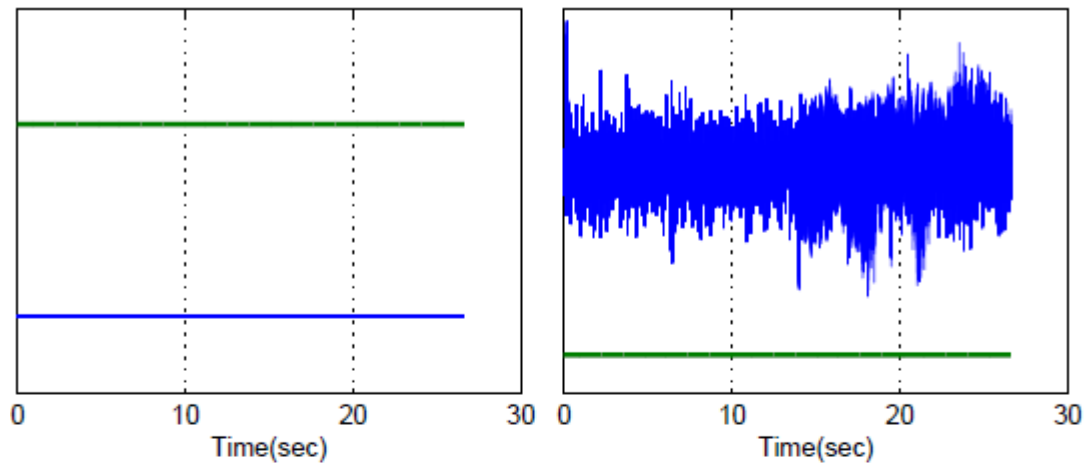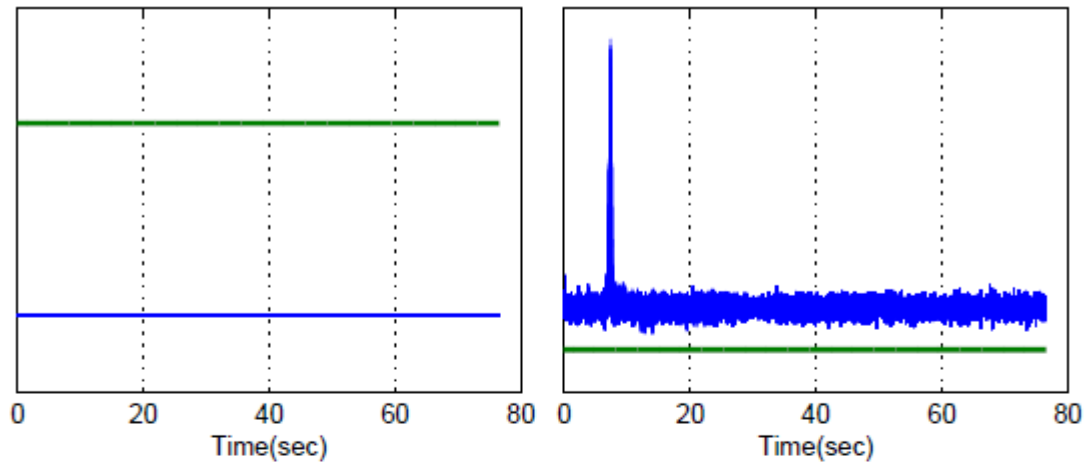
(a) Residuals associated with 'liquid' jamming
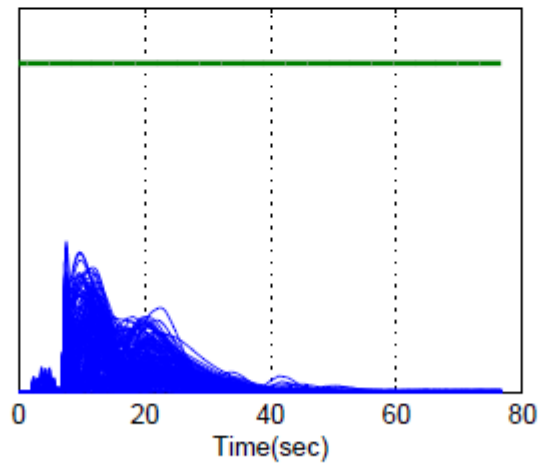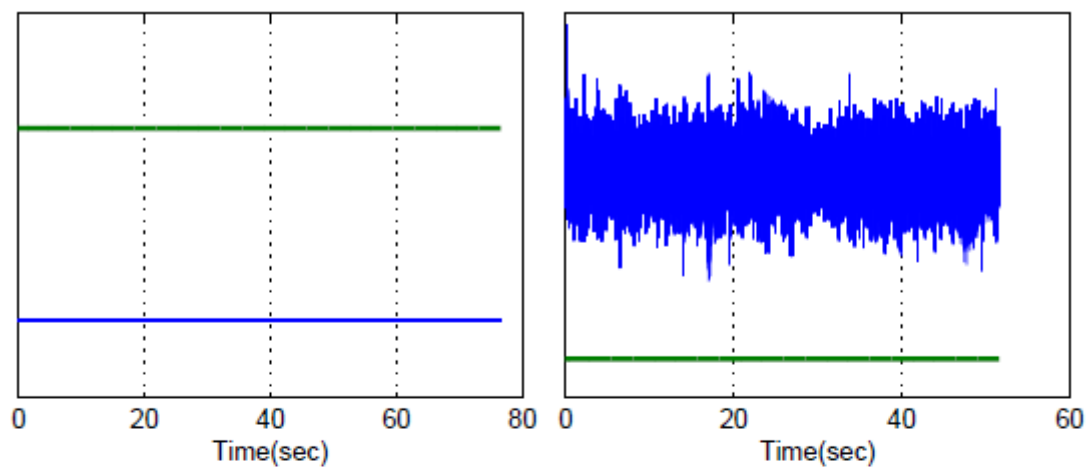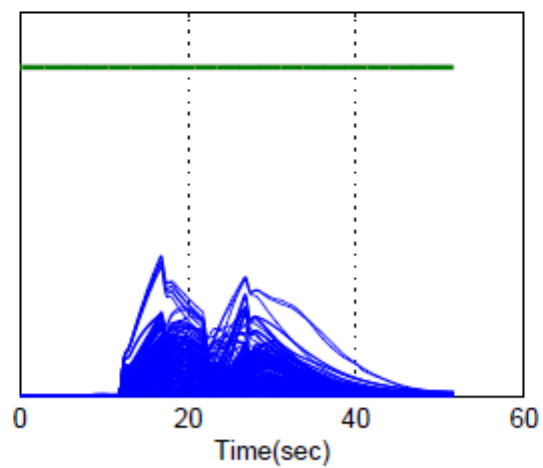
(b) Residuals associated with 'solid' jamming
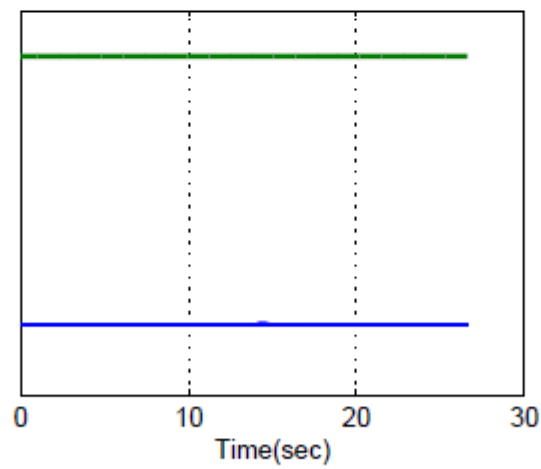
(c) Residuals associated with surface disconnection

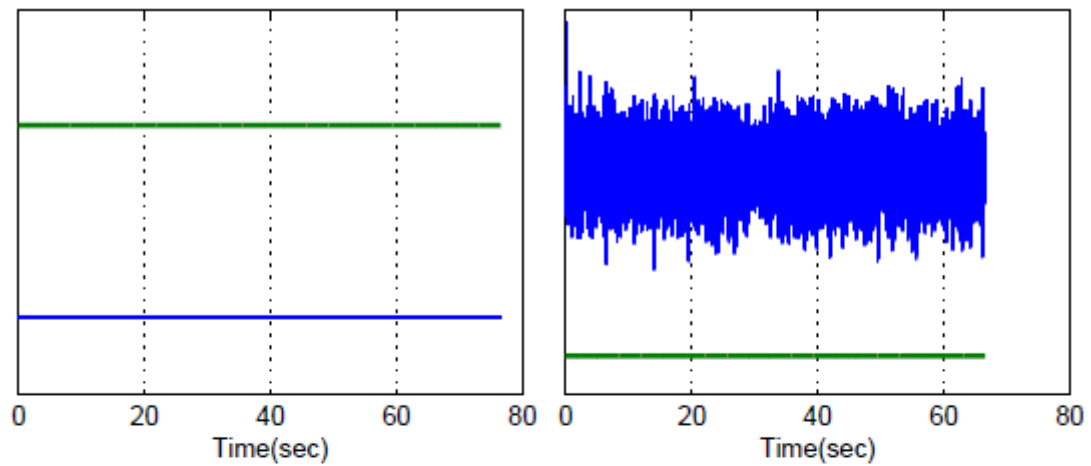Figure 3: Residuals during Nose up in fault free case
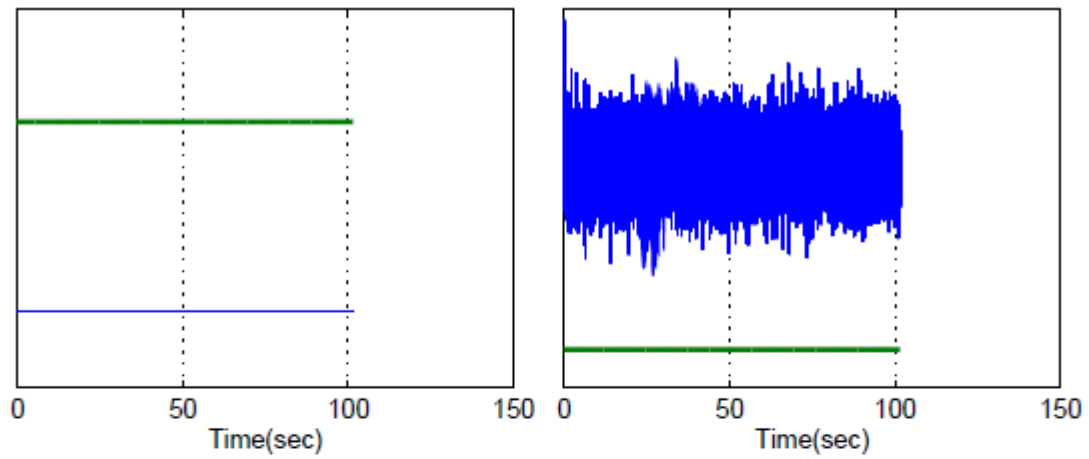
(a) Residuals associated with 'liquid' jamming

(b) Residuals associated with 'solid' jamming
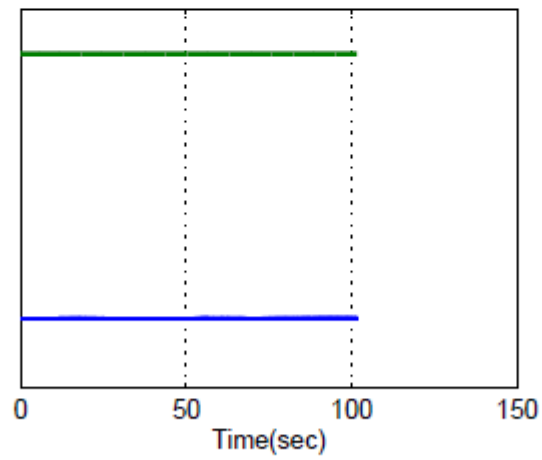
(c) Residuals associated with surface disconnection

Figure 4: Residuals during Angle of attack (AOA) protection in fault free case
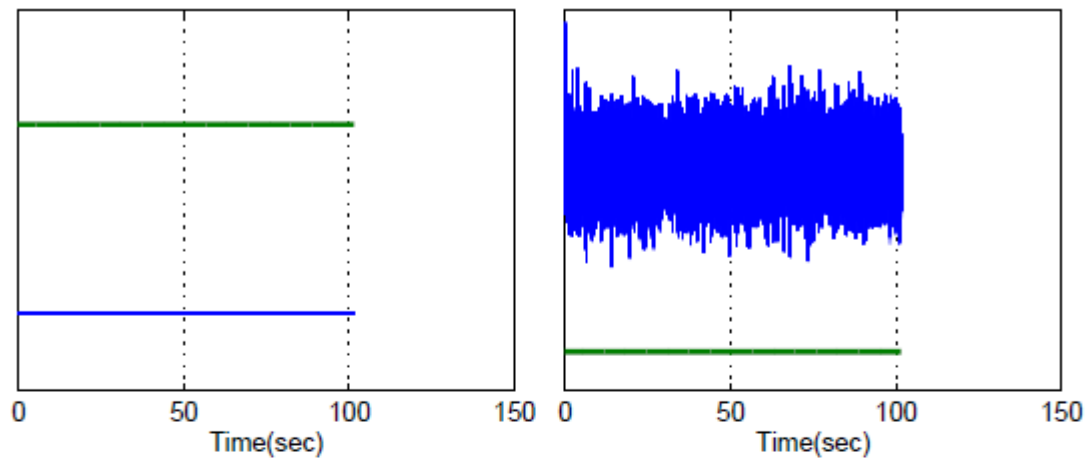
(a) Residuals associated with 'liquid' jamming

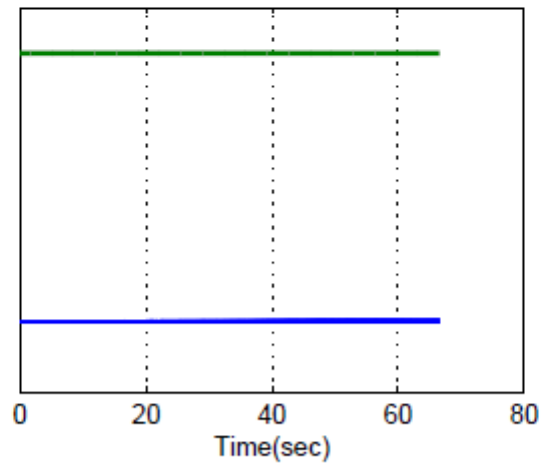(b) Residuals associated with 'solid' jamming
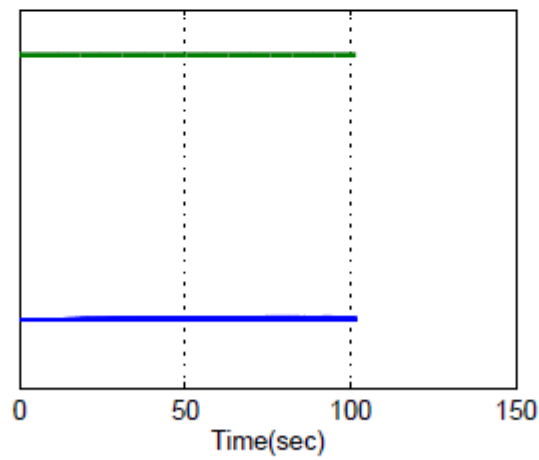
(c) Residuals associated with surface disconnection

Figure 5: Residuals during Pitch protection in fault free case

(a) Residuals associated with 'liquid' jamming

(b) Residuals associated with 'solid' jamming

(c) Residuals associated with surface disconnection

Figure 6: Residuals during Yaw angle mode in fault free case

(a) Residuals associated with 'liquid' jamming

(b) Residuals associated with 'solid' jamming

(c) Residuals associated with surface disconnection

Figure 7: Residuals during Turn coordinate in fault free case

(a) Residuals associated with 'liquid' jamming

(b) Residuals associated with 'solid' jamming

(c) Residuals associated with surface disconnection

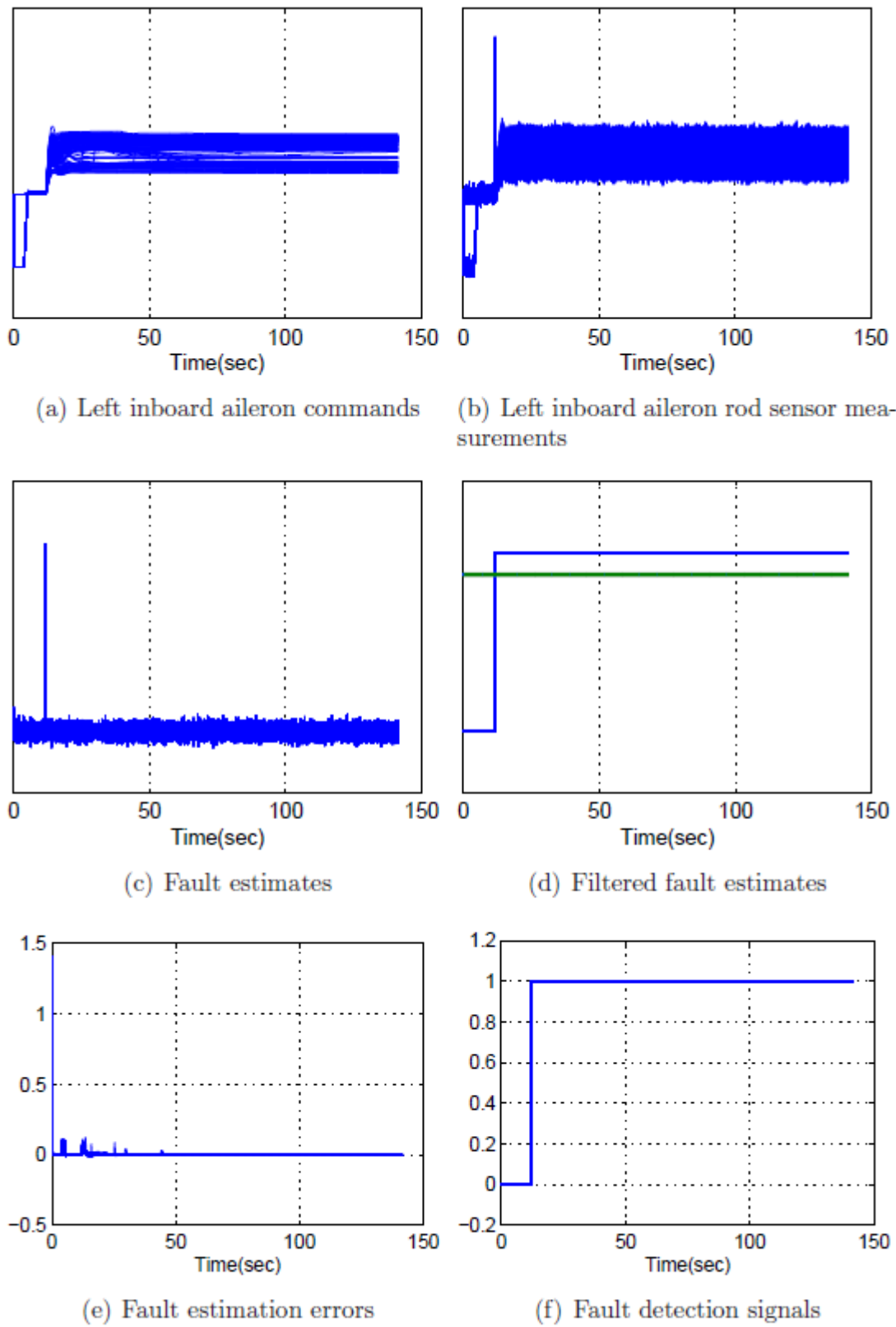Figure 8: Residuals during Cruise in fault free case

(a) Left inboard aileron commands

(b) Left inboard aileron rod sensor measurements

(c) Fault estimates

(d) Filtered fault estimates

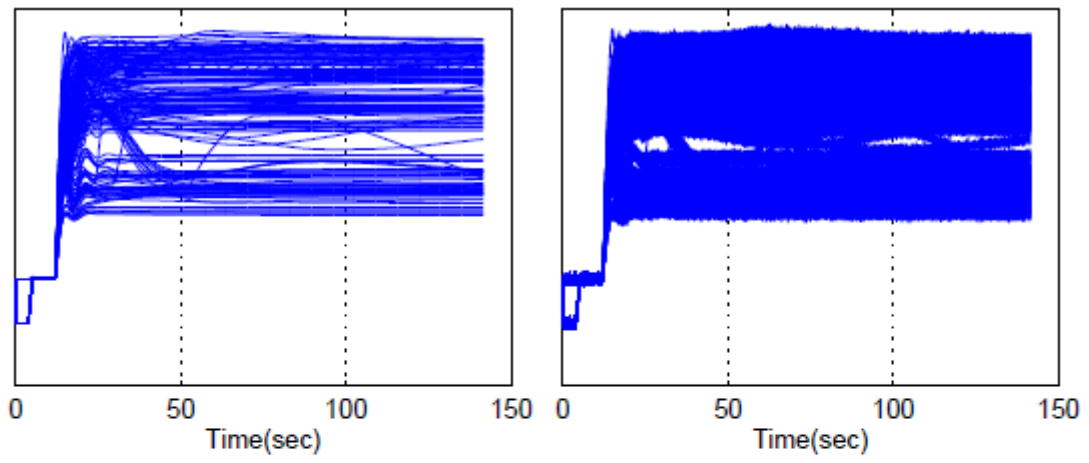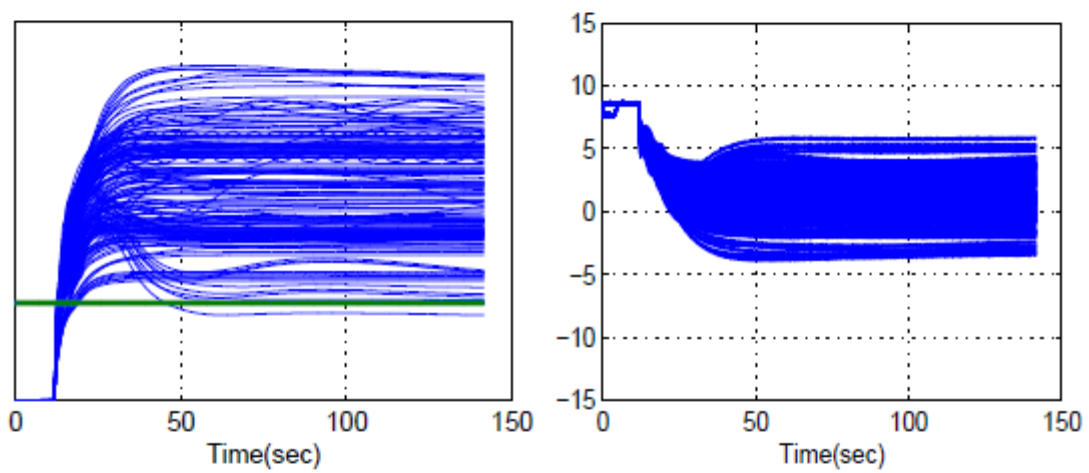(e) Fault estimation errors

(f) Fault detection signals

Figure 9: Fault estimation performance in the presence of 'liquid' jamming

(a) Left inboard aileron commands

(b) Left inboard aileron rod sensor measurements

(c) Fault estimates

(d) Fault estimation errors

(e) Fault detection signals
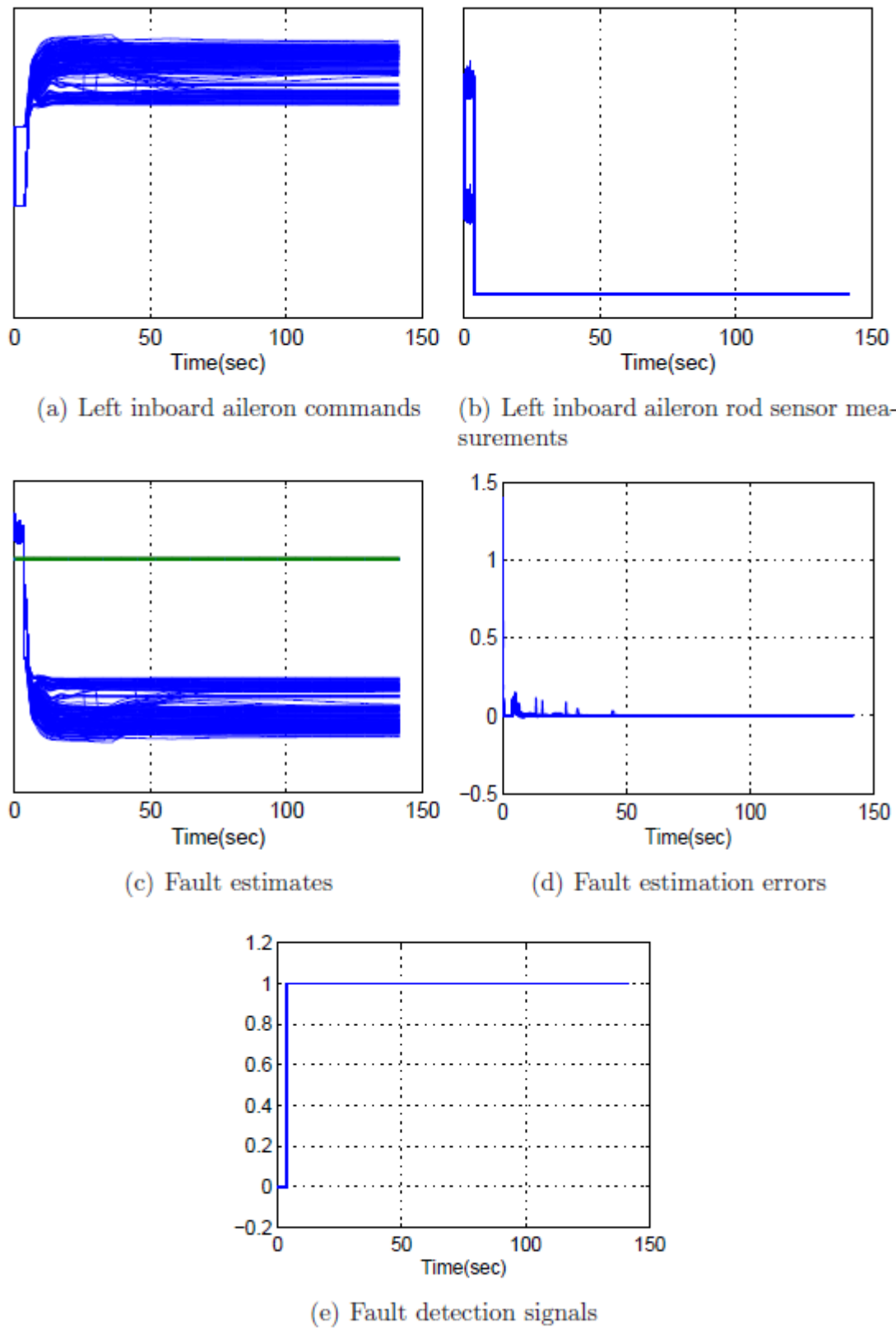
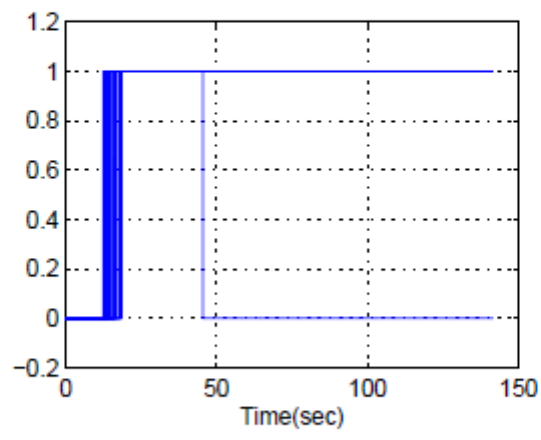Figure 10: Fault estimation performance in the presence of 'solid' jamming

(a) Left inboard aileron commands

(b) Left inboard aileron rod sensor measurements

(c) Fault estimates

(d) Fault estimation errors

(e) Fault detection signals

Figure 11: Fault performance in the presence of the surface disconnection